Imaging Biomarkers of Angiogenesis and the Microvascular Environment in Cerebral Tumors

15

Alan Jackson, Ibrahim Djoukhadar, and David J. Coope

Contents

A. Jackson (✉) • I. Djoukhadar • D.J. Coope
Wolfson Molecular Imaging Centre, University of Manchester, Withington, Manchester, UK
e-mail: Alan.Jackson@manchester.ac.uk; Ibrahim.Djoukhadar@Manchester.ac.uk; david.coope@manchester.ac.uk

L. Saba, E. Raz (eds.), *Neurovascular Imaging*,
DOI 10.1007/978-1-4614-9029-6_18

Abstract

The structure and organization of blood vessels within tumor tissue is very different from that seen in normal tissues. Tumor blood vessels show abnormalities in microstructure and hierarchical organization, which result from multiple factors including local tumor characteristics, angiogenic drive, and the ability of the angiogenic process to keep pace with tumor growth. Tumor microvasculature is inefficient compared to that seen in normal tissues, and, particularly in rapidly growing tumors, blood flow is often inadequate to meet the demands for oxygen and nutrient delivery and clearance of waste material. Understanding the microvascular environment and its variation between and within tumors is critical for an understanding of tumor behavior and therapeutic response. A wide range of quantitative imaging techniques have been developed in an attempt to provide noninvasive, repeatable assays of microvascular characteristics which can then be studied in terms of their spatial variability and change over time. This chapter reviews the currently available imaging biomarkers and their current clinical application.

Keywords

Angiogenesis • Blood vessels • Permeability • Flow • Dynamic contrast-enhanced imaging • Positron emission tomography • Hypoxia • Integrins

Introduction

The development of new blood vessels (angiogenesis) is an essential component of tumor growth and is one of the classic hallmarks of the cancer cell [1]. The development of new blood vessels, their maturation, and organization give rise to a distinctive vascular microenvironment that has been shown to vary significantly between tumor types and even within individual tumors. The characteristics of the vascular microenvironment will place constraints on the delivery of nutrients, oxygen, and drugs as well as the distribution of macromolecules, which can in turn directly affect the behavior of tumor cells. The development of therapeutic approaches, which target the angiogenic process or the neovasculature, has led to enormous research activity in this area over the past 20 years. Imaging techniques have been widely applied to study the process of angiogenesis and the characteristics of the tumor vascular microenvironment (TVM). Imaging has unique strengths allowing repeated, noninvasive assessment of the whole tumor or multiple tumors in the same patient. In addition, imaging provides spatial data allowing the study of regional variations in the microenvironment within a single tumor. Imaging also allows the development of quantitative metrics, which reflect the physiological, pharmacological, or pathological processes occurring within the tumor. Such quantitative metrics are referred to as imaging biomarkers (IB), and considerable research activity has been focused on the discovery, technical, and biological validation of IB that allow characterization of the TVM. In this chapter, the characteristics of the TVM and the IB available for its characterization and their current applications are reviewed.

Abnormalities of Tumor Blood Vessels

In normal tissues a single layer of endothelial cells (EC) lines blood vessels forming a barrier limiting the passage of macromolecules. EC are surrounded by tightly connected pericytes and both of these enveloped in a basement membrane. In normal tissues pericytes are heavily involved in the suppression of EC proliferation and EC are quiescent, showing no evidence of division or sprouting of new vessels [2]. Pericytes produce a number of signaling molecules, which include vascular endothelial growth factor (VEGF), angiopoietin-1 (Ang-1), fibroblast growth factors (FGFs), NOTCH, and chemokines, which support normal endothelial cell repair. Endothelial cells can also respond directly to dissolved oxygen concentration and have receptors for hypoxia-inducible factors such as prolyl-hydroxylase domain 2 (PHD2) and hypoxia-inducible factor-2α (HIF-2α) which support mechanisms to enable

remodeling of vessels to optimize oxygen delivery. Within normal tissue blood vessels are arranged in a clear hierarchy, with inflow of blood managed by arterial vessels and branching arterioles feeding a capillary network, which drains into venules and larger veins. These vascular networks vary from tissue to tissue but are, in general, highly structured and internally consistent.

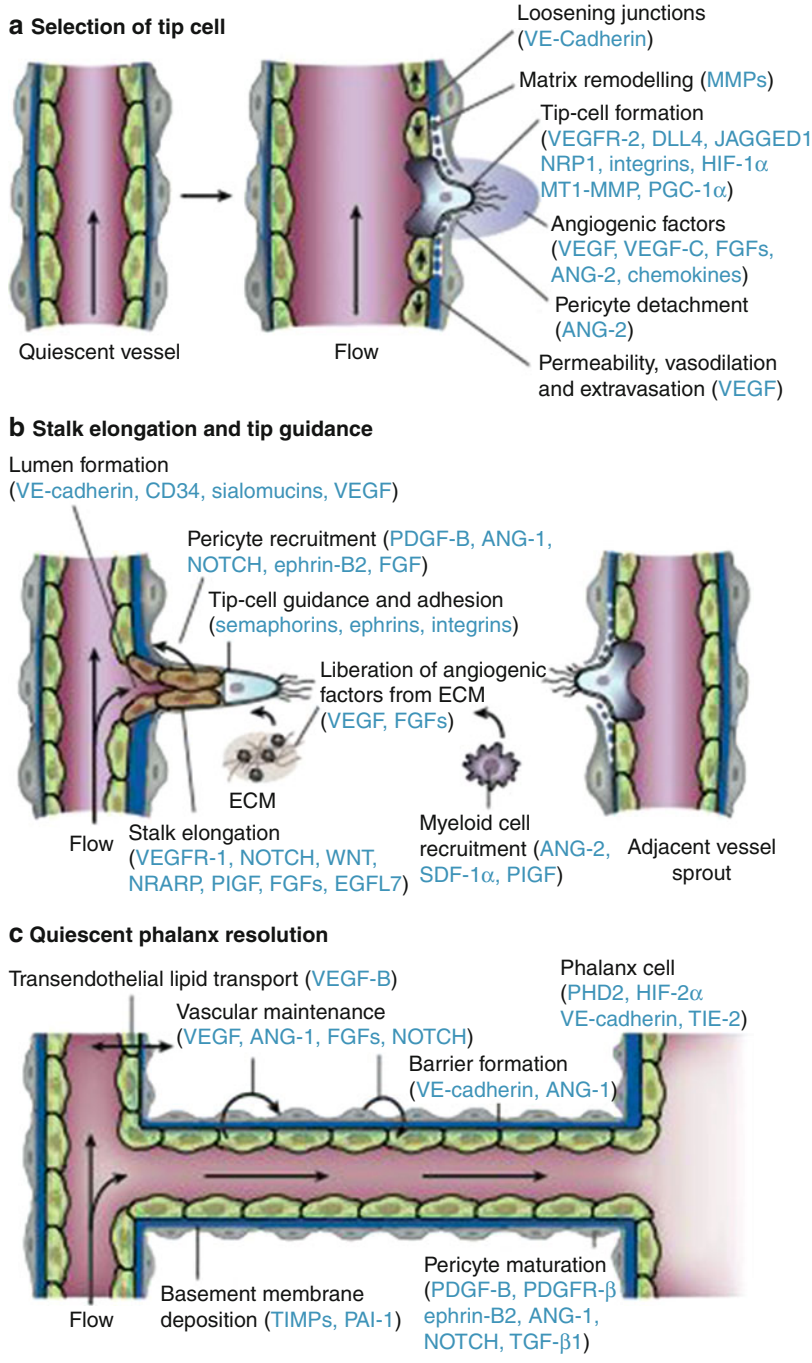

Fig. 1 (continued)

Tumor vasculature demonstrates a wide range of abnormalities dependent on the tumor type. As tumors develop, they depend on the development of new blood vessels to meet increasing demand for nutrient delivery and waste removal. This process of neovascularization is referred to as angiogenesis [2]. Angiogenesis is controlled by a number of signaling mechanisms mediated by small molecules known as cytokines which may be released from tumor cells, EC, hypoxic normal cells, or inflammatory tissue [3]. In normal tissue the angiogenic process forms a normal part of development [2]. In tumors, the presence of hypoxia and hypoglycemia promotes the release of pro-angiogenic signaling molecules including VEGF, Ang-2, FGFs, and chemokines into the local microenvironment. In normal vessels exposed to these pro-angiogenic stimuli, pericytes detach from the basement membrane under the action of matrix metalloproteinases (MMP) and the tight junctions between endothelial cells loosen, increasing the permeability of the endothelial membrane (Fig. 1).

Plasma proteins extravasate into the extravascular space and form an early extracellular matrix, while integrin signaling stimulates migration of EC onto the matrix. New vessels grow in an ordered process that involves migration of a single EC, known as the tip cell along the new matrix. Nearby EC, known as stalk cells, divide to form an elongated vascular core that then develops a patent lumen in response to a range of signaling molecules. These new vessels fuse with existing ones to initiate blood flow and, in time, develop a pericyte coverage. As they mature they may reform EC tight junctions and basement membranes.

In general terms, rapidly growing aggressive tumors provide greater angiogenic drive and will result in increasingly disordered microvascular environments. In some, slowly growing, tumors such as low-grade meningiomas, the microvascular architecture can be remarkably structured with well-developed hexagonal arteriolar and capillary territories clearly seen. In more aggressive tumors such as glioma, tumor vessels are disorganized, irregular, and tortuous with bizarre branching patterns. They do not maintain the normal arterial/capillaries/venous hierarchy and all components of the tumor vessel wall are abnormal. EC tight junctions are absent, rendering tumor vessels leaky to macromolecules and often with a propensity to microhemorrhage. These neovascular structures are dynamic, showing constant changes in blood vessel development and variations in hemodynamics so that blood flow in individual regions may change in volume and direction even over short time periods. Primary malignant brain neoplasms exhibit the greatest degree of vascular proliferation of any tumor type, and angiogenesis is a key step in their progression [4].

Fig. 1 The consecutive steps of blood vessel branching are shown, with the key molecular players involved denoted in parentheses. (**a**) After stimulation with angiogenic factors, the quiescent vessel dilates and an endothelial tip cell is selected (DLL4 and JAGGED1) to ensure branch formation. Tip-cell formation requires degradation of the basement membrane, pericyte detachment, and loosening of endothelial cell junctions. Increased permeability permits extravasation of plasma proteins (such as fibrinogen and fibronectin) to deposit a provisional matrix layer, and proteases remodel preexisting interstitial matrix, all enabling cell migration. For simplicity, only the basement membrane between endothelial cells and pericytes is depicted, but in reality, both pericytes and endothelial cells are embedded in this basement membrane. (**b**) Tip cells navigate in response to guidance signals (such as semaphorins and ephrins) and adhere to the extracellular matrix (mediated by integrins) to migrate. Stalk cells behind the tip cell proliferate, elongate, and form a lumen, and sprouts fuse to establish a perfused neovessel. Proliferating stalk cells attract pericytes and deposit basement membranes to become stabilized. Recruited myeloid cells such as tumor-associated macrophages (TAMs) and TIE-2-expressing monocytes (TEMs) can produce pro-angiogenic factors or proteolytically liberate angiogenic growth factors from the ECM. (**c**) After fusion of neighboring branches, lumen formation allows perfusion of the neovessel, which resumes quiescence by promoting a phalanx phenotype, reestablishment of junctions, deposition of basement membrane, maturation of pericytes, and production of vascular maintenance signals. Other factors promote transendothelial lipid transport (From Ref. [3] with permission)

Most tumors have far less blood flow than would be expected from their vascularity, reflecting the inefficiency of the tumor vasculature. In addition, leakage of large molecules and the lack of normal lymphatic drainage can result in high interstitial pressures, which further impair regional perfusion. Consequently, regional hypoxemia and necrosis are common, particularly in aggressive tumors.

Antiangiogenic Therapies

The ubiquitous nature of the angiogenic process led to great excitement in the 1990s with the hope that therapeutic approaches, which targeted pathological angiogenesis, would provide a "magic bullet" that could be used to deprive a large range of tumors of the blood vessels necessary for development and expansion. The development of antiangiogenic drugs and of antivascular agents, which target abnormal, developing vessels, led to one of the most extensive areas of anticancer research in recent decades. Despite this, antiangiogenics, while showing efficiency as single or combination agents in a number of tumor types, have failed to provide the prolonged tumor suppression of tumor activity commonly observed in animal models. Many mechanisms have been identified which imbue tumor cells, EC, or other components of the tumor stroma with resistance to angiogenic inhibition, and some agents have proven toxic when combined with chemotherapy [5]. Compensatory increase in other pro-angiogenic signaling pathways can support tumor angiogenesis independently from VEGF, and some evidence is beginning to suggest that antiangiogenic therapy may cause cancer cells to become increasingly malignant in behavior. Secondary hypoxia can induce mutations resulting in hypoxic-resistant tumor cells and alternate pro-angiogenic "escape" mechanisms. In glioma there is also evidence that EC can be formed from primary tumor stem cells via a process that is relatively insensitive to blockade of VEGF. While the lack of curative single-agent efficiency is disappointing, it is clear that antiangiogenic agents offer significant survival benefit in combination therapies and research into this mechanism of drug action continues, albeit with new expectations. The main questions which now face imaging researchers in this field are more demanding and include: Can IB predict therapeutic response to specific agents or combination therapies? Can IB guide selection of optimal therapeutic combinations? Can IB be used to optimize the timings of combination therapies? Can IB identify and/or predict specific mechanisms of resistance and appropriate subsequent interventions?

Imaging the Tumor Vascular Microenvironment

It is clear that the TVM represents one of the most profoundly important factors both in tumor behavior and therapeutic response. It controls the ability of individual regions of proliferating tumor cells to obtain sufficient nutrients and oxygen. Failure of vascular development, adequate to the requirements of the developing tumor, results in regional hypoxia with the consequent effects on local tumor and blood vessel growth and a drive toward genotypic instability and tumor cell mutation. It can also result in regional necrosis and tumor cell death. Features of the TVM also control the passage of macromolecules and inflammatory cells into the tissue and the generation of hematogenous metastatic deposits. The ability to study and measure these biological processes is essential, and many can be characterized and quantified in exquisite detail on the basis of tissue biopsy or even by examination of circulating tumor cells and soluble biomarkers. Despite this, imaging techniques remain the only available approach to studying the TVM in situ without the need for biopsy or surgical resection. Furthermore, imaging techniques support studies of the entire tumor, can provide information on the heterogeneity of individual biological features, and can, in many cases, be optimized to provide biological data of direct relevance to tumor biology. These features, together with the minimally invasive nature of

most imaging techniques and the ability to repeat studies whenever necessary, give imaging significant advantages over other methodological approaches.

In recent years, the concept of the imaging biomarker (IB) has become the basis for the development of novel imaging methods. A biomarker is defined as "a quantitative parameter which directly reflects the physiology, anatomy or pathological process under investigation." The use of soluble and tissue biomarkers, like prostate-specific antigen or CA 125, has led to the development of "biomarker roadmaps" designed to standardize the discovery, technical, and biological validation of individual biomarkers to ensure that they are fit for purpose. The concept of an IB is identical and requires identification of a potentially valuable, measurable imaging feature, proof that it is technically measurable in single or multi-institutional settings, characterization of its repeatability and reproducibility, and evidence to support its biological validity. For imaging techniques the technical validation steps are often more extensive than those required for soluble and tissue biomarkers and can be technically challenging, particularly where imaging techniques must be standardized across different manufacturers, imaging platforms, and institutions. Despite this, the development of novel IB now forms one of the main areas of imaging research both in cancer and other diseases.

In the remainder of this chapter, the IB available for quantified imaging of the TVM is reviewed, the evidence for their technical and biological validity is discussed, and their applications to the present time are reviewed.

Imaging Biomarkers

The development of IB to characterize the tumor microenvironment and the angiogenic process has been and continues to be a major area of imaging research. All major modalities have been utilized, including CT, MR, single-photon emission computed tomography (SPECT), positron emission tomography (PET), ultrasound, and optical imaging. The last two are largely experimental, being used primarily in the intraoperative setting or in animal models of disease, and will not be discussed further.

Most early imaging studies focused on the characterization of aspects of the TVM involved in the angiogenic process, specifically the amount of blood vessels and the increases in capillary endothelial permeability induced by pro-angiogenic cytokines. Both of these features can be estimated using dynamic contrast-enhanced imaging techniques, which are now widely employed both in clinical practice and in trials of antiangiogenic and vascular targeting agents. However, more recently there has been significant interest in developing biomarkers that target other aspects of the TVM, leading to the description of an increasingly wide range of IB and, in particular, of PET-based molecular imaging agents.

Biomarkers of Perfusion and the Vascular Microenvironment

The early development of IB for tumor microvascular structure focused on attempts to measure the known histological features of angiogenic tissue. Classically, histochemical staining studies had identified the importance of the density of new vessels (microvascular density; MVD) measured on stained tissue. MVD has been shown to relate to malignancy and outcome in a number of tumors and is routinely used in histological studies [6]. It was quickly realized that a theoretical surrogate of MVD could be extracted from dynamic contrast-enhanced MRI.

Dynamic Susceptibility Contrast-Enhanced MRI (DSCE-MRI)

Early studies concentrated on the use of dynamic T2*WI acquisitions, often referred to as Dynamic Susceptibility Contrast-Enhanced MRI (DSCE-MRI), in neoplastic and cerebral vascular disease. The initial focus on DSCE-MRI arose from the fact that system architecture at that time made rapid dynamic acquisitions with T2* star

weighting more straightforward than dynamic T1-WI imaging. More importantly, the signal change in T2*WI images arises from the effects of the locally altered magnetic field which extends some distance from the contrast molecule. In isolated capillary beds this means that signal is generated from protons within the extravascular extracellular space (EES), even if contrast molecules remain entirely intravascular. This susceptibility effect gives rise to slightly higher proportional signal changes in the normal gray and white matter which is a significant advantage in normal cerebral capillary beds. The analysis of the dynamic signal intensity time course curves (SI-TCC) from DSCE-MRI is also relatively straightforward. Dynamic time course signal changes can be transformed into estimates of contrast concentration time course curves (CAA-TCC) from which estimates of proportional cerebral blood volume can be derived as the area under the contrast agent concentration curve during its first passage. This area correlates with the proportion of the volume of the voxel filled by blood vessels often referred to as the relative cerebral blood volume (rCBV). By scaling to normal white matter or pure vascular tissues (large veins), rCBV can be normalized to produce absolute values (CBV), which have shown close agreement with histological assessment of MVD in a number of cancer types and show similar correlations with tumor grade, aggressiveness, and survival data [7].

The basic analysis approaches for the DSCE-MRI assumed that contrast agent remains intravascular in the presence of an intact blood–brain barrier. In tumor tissue this causes very significant errors since contrast agent leakage into the EES produces contradictory signal changes, due to T1 effects. These give rise to artificially low estimates of CBV (so-called T1 shine through). These leakage errors can be reduced by preloading the tissue with a dose of contrast agent prior to the dynamic contrast study, by the use of low flip angle sequences with low T1 sensitivity, or by signal post-processing [8]. Increasingly, contrast agent preloading, signal processing, or a combination of the two is routinely used. The use of low flip angle acquisition sequences has been relatively unpopular since, although these do abrogate the effect of the so-called T1 shine through signal, they also result in significant decreases in signal-to-noise ratio with consequent reductions in the accuracy of subsequent curve fitting analyses.

The growing application of DSCE-MRI in neuro-oncology led to a number of additional analytical approaches designed to provide additional data about the TVM. It was rapidly realized that in tumor vasculature, the normal shape of the CC-TCC was distorted by retention of contrast agent following the first passage of the contrast bolus. This elevation of contrast concentration was first described as the relative recirculation (rR) parameter and has also been widely referred to as the percentage recovery (describing the percentage of signal recovery to the baseline). This has been variously attributed to contrast linkage and to retention of contrast agent within the abnormal microvasculature due to vessel tortuosity and regional reductions in perfusion pressure. These metrics allow identification of areas of tumor where capillary flow is present, but delayed, corresponding to regions with reduced perfusion pressure and reduced flow and has been used to differentiate GBM from metastasis [9].

The development of more complex image analysis techniques led to the development of pharmacokinetic models designed with the intention of measuring regional blood flow and/or capillary endothelial permeability. These approaches require correction of the tissue residue function from the individual tumor voxels to correct for variations in the width of the injected arterial bolus, known as the arterial input function (AIF). Correcting for the variation between patients resulting from individual variations in AIF allows estimations of regional capillary blood flow. Unfortunately, the accuracy of these estimates is greatly affected by delays in the arrival of the contrast bolus within the tissue and by variations in dispersion of the contrast bolus, which result from a combination of flow delays and irregular vessel flow patterns. The result of these effects is that regional capillary flow estimates can only be acquired reliably where there can be an assumption of normal arterial/capillary/venous hierarchy, which is not the case in tumor tissue [10].

Most early antiangiogenic agents targeted VEGF or VEGF signaling. Since VEGF produces rapid and significant increases in the permeability of the endothelial membrane, considerable work was directed toward the quantification of permeability by measurement of MR contrast agent leakage. Analysis of DSCE-MRI using a two-compartment leakage model was described in an attempt to estimate permeability surface area product of the local tumor capillary bed. These pharmacokinetic analysis techniques allow estimation of the contrast transfer coefficient (K^{trans}) between the plasma and extravascular extracellular space (EES). However, modeling of leakage effects using T2* dynamic images is challenging, and attention rapidly shifted to the use of T1-WI dynamic acquisitions.

Dynamic Relaxivity Contrast-Enhanced MRI (DRCE-MRI)

On T1-WI images, signal change observed in response to intravascular and extravascular contrast agent is additive, simplifying attempts to estimate the magnitude of contrast agent leakage in comparison to DSCE-MRI. Furthermore, the majority of clinical MR scanning systems are capable of acquiring DRCE-MRI data. DRCE-MRI data can be analyzed using simple semiquantitative metrics, although in research applications these have commonly been avoided since intensity changes can vary between systems due to differences in acquisition sequence design, receiver gain settings, and other technical variables. Early studies attempted to minimize these sources of variation by the use of simple, normalized, metrics such as the maximal rate of change of signal intensity or the ratio of pre- and postcontrast signal intensity. Subsequent improvements in hardware and particularly in gradient coil design have minimized variations in observed signal change, and these together with the use of normalized metrics have led to routine clinical use of semiquantitative measurements in prostate, breast, pancreatic, cervical, colonic, and rectal cancers, bone sarcoma, as well as brain tumors. The clinical preference for semiquantitative metrics reflects the complexity of pharmacokinetic approaches and the lack of available standardized software for clinical application (Fig. 2) [11].

Despite this a desire for better standardization across imaging systems and for greater physiological specificity led to the development and widespread application of pharmacokinetic analytical approaches [12].

Pharmacokinetic analysis of DRCE-MRI data requires transformation of signal change measurements into estimates of contrast agent concentration to allow the measurement of CC-TCC (Fig. 3).

This can be performed assuming that the baseline T1 values of the tissue are measured prior to contrast agent administration. While accurate measurement of T1 values can be time-consuming, the use of multiple flip angle gradient echo sequences produces adequate accuracy in acceptable acquisition times and has become routine. Analysis of the CC-TCC can then be undertaken using a variety of pharmacokinetic distribution models. All of these models require provision of an explicit input function representing the arterial input to the tissue (AIF). The accuracy of measurement of AIF has a considerable effect on the accuracy of derived values of parameters from the analysis, and many authors have studied the optimal sampling and modeling of the AIF. Where an AIF cannot be measured with sufficient accuracy, then a population-based AIF may be applied.

The most common pharmacokinetic analysis approach is a modified version of the original Toft's pharmacokinetic model that produces estimates of vascular fraction (v_p), extravascular extracellular space fraction (v_e), and the transfer contrast coefficient (K^{trans}) [14]. The K^{trans} parameter is widely used in DRCE-MRI studies, often as a potential surrogate of capillary endothelial permeability. However, although K^{trans} will be affected by the permeability, it is a bulk transfer coefficient, so that it is also affected by the surface area of the capillary endothelial bed and by rate of delivery. This means that in very low flow states, particularly where leakage is high, the transfer coefficient will depend almost entirely on flow, whereas in high flow states with low permeability, it will depend almost entirely on permeability. Nonetheless it rapidly became evident that the VEGF inhibition was indeed associated with rapid and

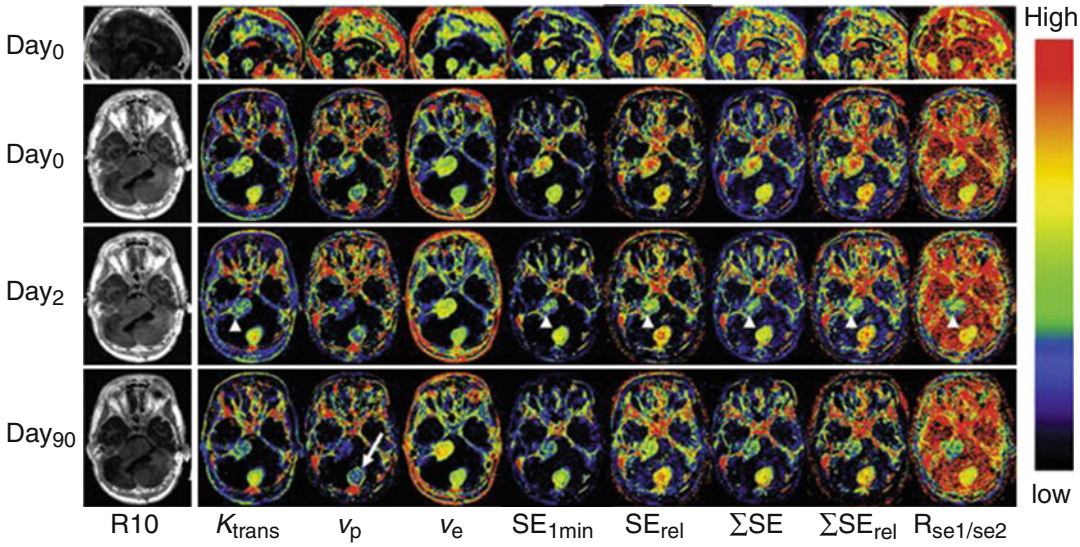

Fig. 2 Axial view of central slices of 3D longitudinally co-registered kinetic and semiquantitative parametric maps obtained in a 26-year-old woman, who has Type II neurofibromatosis with a progressive VS (*arrow heads*) and an occipital located meningioma (*arrow*) undergoing treatment with bevacizumab. Images show comparisons of pharmacokinetic leak derived parameters Ktrans, vp, and ve with semiquantitative parameters: (1) *absolute signal enhancement* (SE_{1min}), (2) *relative signal enhancement* (SE_{rel}) which uses a baseline value for normalization in order to reduce the dependence on biological and imaging system variables, (3) *the sum of SE over a fixed post-injection duration* (SE), (4) *the sum of* SE_{rel} *over a fixed post-injection duration* (SE_{rel}), and (5) *signal enhancement ratio*, commonly defined as the ratio of early to late contrast enhancement ratio, e.g., $R_{se1/se2} = \left(SI_{1min\ post} - SI_{pre}\right) / \left(SI_{5min\ post} - SI_{pre}\right)$ (From Ref. [11] with permission)

profound reductions in K^{trans} [13]. Although the modified Toft's model has been widely used, a variety of alternate pharmacokinetic models exist, ranging from simple two-compartment models, such as the original Toft's model, to more complex models, such as the adiabatic tissue homogeneity model, where more specific physiological information is sought by definition of additional biological variables (Table 1).

The choice of appropriate pharmacokinetic models depends on a wide range of factors. In some instances the demands of an individual study may require absolute estimation of physiological variables such as regional capillary blood flow (F) which can be provided only by more complex models. In contrast, the use of increasingly complex models introduces uncertainty into parameter estimates due to the need to optimize to an increasing number of variables. This in turn places significant demands on the image acquisition strategy requiring high temporal resolution data with high signal-to-noise characteristics. The need to "square the circle" by producing very high spatial resolution data with high temporal resolution measurement of the AIF and high signal-to-noise characteristics has led to extensive research into MR image acquisition leading to a number of novel fast image acquisition approaches for DCE-MRI and the development of dual injection methods where separate dynamic acquisitions are acquired to provide matched high spatial and high temporal resolution data.

Dynamic Contrast-Enhanced Computed Tomography (DCE-CT)

With the development of rapid multi-slice CT acquisitions, it was natural that the analytical approaches taken with DCE-MRI would be applied to CT data. Dynamic CT (DCT) has a number of potential advantages over MRI. The

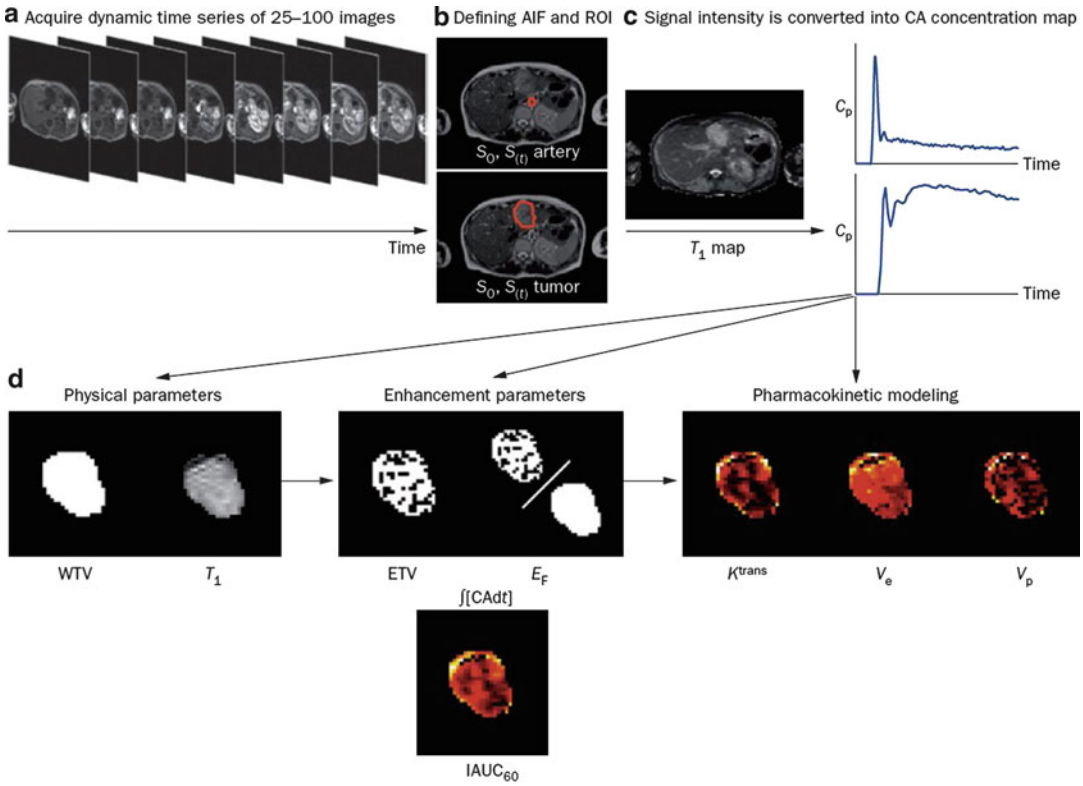

Fig. 3 DCE-MRI data acquisition and analysis. (**a**) Multiple images (typically 25–100) are acquired as a bolus of contrast agent passes through tissue capillaries; (**b**) the region of interest for a tumor and the feeding vessel arterial input function are defined; and (**c**) signal intensity values for each voxel are converted into contrast agent concentration using a map of T1 values. These steps allow calculation of (**d**) WTV and T1 values. Next, voxels are classified as enhancing or not after which parameters based on the amount and proportion of enhancement can be defined, along with the IAUC60. Finally, a pharmacokinetic model may be applied to derive parameters such as Ktrans. Abbreviations: *∫[CA]dt* area under the contrast agent–time curve, *AIF* arterial input function, *Cp* contrast agent concentration in plasma, *CA* contrast agent, *DCE-MRI* dynamic contrast-enhanced MRI, *EF* enhancing fraction, *ETV* enhancing tumor volume, *IAUC60* initial area under concentration agent–time curve at 60 s, *Ktrans* volume transfer constant between plasma and the extracellular extravascular leakage space, *ROI* region of interest, *S* signal, *T1* longitudinal relaxation time, *ve* volume of extracellular extravascular leakage space, *vp* blood plasma volume, *WTV* whole tumor volume (From Ref. [13] with permission)

main one of these is that the concentration of contrast agent is directly linearly related to the measured attenuation value; this makes measurements of semiquantitative parameters and the application pharmacokinetic models more simple and alleviates many of the problems associated with multicentered studies in MRI [16]. The main problem with DCT is of course the radiation dose, which is significant and limits the application of the technique into clinical trials requiring repeated imaging measurements.

Imaging Microvessel Morphology and Hypoxia with MRI

Vessel Size Imaging (VSI) and Vessel Architectural Imaging (VAI)

As described above, a great deal of the development of dynamic contrast-enhanced techniques arose from a desire to study changes in regional blood volume or capillary endothelial permeability. An important feature of antiangiogenic

Table 1 Parameters derived in DCE-MRI

Parameter	Definition	Unit	Notes
Primary end points[a]			
K^{trans}	Volume transfer constant between plasma and the EES	min^{-1}	Composite measure of permeability, capillary surface are and flow
$IAUC_{60}$	Initial area under concentration agent-time curve at 60 s	mmol min	Similar measure to K^{trans}, but also influences by V_e
Alternative functional biomarkers[b]			
k_{ep}	Rate constant between EES and plasma	min^{-1}	NA
V_e	Volume of EES per unit volume of tissue	NA	NA
V_p	Blood plasma volume	NA	Relatively poor reproducibility
F	Blood flow	ml/ g min^{-1}	Temporal resolution achieved in most studies s too slow
PS	Permeability surface area product per unit mass of tissue	ml/ g min^{-1}	Temporal resolution achieved in most studies is too slow
Alternative biophysical measurements[c]			
WTV	Whole tumor volume	mm^3	Easy to measure
ETV	Enhancing tumor volume	mm^3	Easy to measure
E_F	Enhancing fraction (ETV:WTV ratio)	none	Easy to measure
T_1	Longitudinal relaxation time	ms	Easy to measure

DCE-MRI dynamic contrast-enhanced MRI, *EES* extracellular extravascular leakage space, *NA* not applicable
[a]As recommended by Leach et al. [15]
[b]Require pharmacokinetic modeling
[c]Do not require pharmacokinetic modeling

therapy includes reduction in the abnormal tumoral vasculature to produce the so-called "normalization" of vascular structures. This normalization process is characterized by a reduced number of vessels of increasingly normal caliber and reestablishment of the arterial/capillaries/venous hierarchy [17]. As discussed above the signal changes resulting from T1 and T2* relaxation measurements differ significantly. One principal difference is that the relaxivity effect, which produces the reduction in T1, is limited to the immediate spatial environment of the proton, while the variation in local field intensity which results in T2* contrast extends a significant distance beyond the proton, affecting not only the vessels containing contrast but also the surrounding tissue. As a consequence of this difference in the contrast mechanisms, it is possible to model the effect of vessel size and vessel distribution and, using paired T1 and T2*WI acquisitions, to derive a calculated parameter which reflects average vessel size (Rv) [18]. This technique is referred to as vessel size imaging (VSI). VSI is increasingly employed in research settings and has been used, in drug trials, to demonstrate vessel normalization in response to antiangiogenic therapies (Fig. 4) [20].

More recently this approach has been extended following the realization that the difference in contrast mechanisms between T1 and T2* dynamic acquisitions produces not only the difference in signal intensity but also an apparent temporal variation between the maximal effect of T1- and T2*-based signal changes [21]. Modeling of the temporal discrepancies of these signal changes allows estimation of the homogeneity and direction of flow. Furthermore the signals are differentially affected by oxygen tension so that an estimate of regional oxygen extraction can also be calculated. This technique, known as vessel architectural imaging (VAI), has also been applied in studies of antiangiogenic therapies showing different patterns of change in the early phases of treatment in patients who respond to therapy. VAI has also been used to study patients with glioblastoma treated with cediranib and chemoradiation, demonstrating that increases in perfusion and oxygenation, seen in approximately

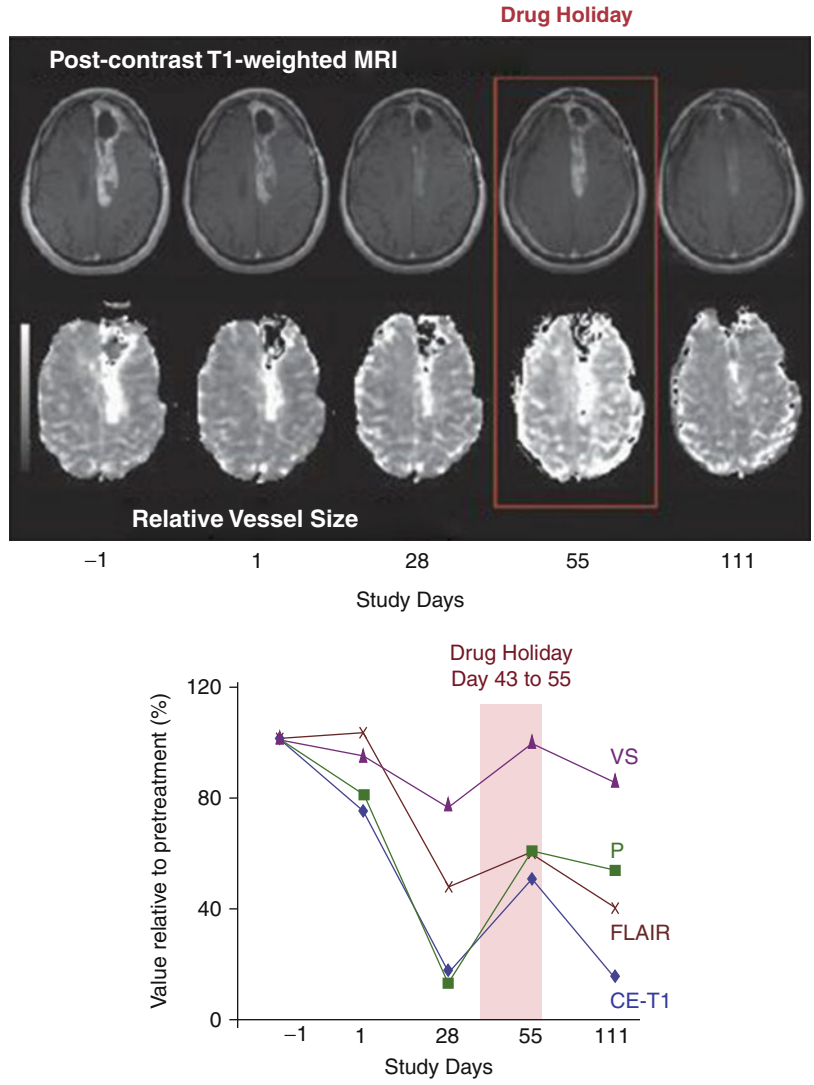

Fig. 4 Reversibility of normalization: (**a**) Vascular and volume changes as a function of time in a patient who did not take drug from days 43 to 56 and was imaged on day 55 (shown as drug holiday). T1-WI anatomic images after intravenous administration of gadolinium-DTPA, similar to Fig. 2. Note that at day 55, there is a rebound in tumor enhancement, which decreases again after restarting the drug as seen on follow-up imaging on day 110. In this patient, maps of relative vessel size (similar to Fig. 1c) also show fluctuation with the drug holiday and resumption of AZD2171 treatment. (**b**) Measurements of imaging parameters confirm the reversibility of vascular normalization by drug interruption followed by renormalization after AZD2171 is resumed (From Ref. [19] with permission)

50 % of patients, are associated with improved survival. In comparison an increase was seen in only one of 14 patients with GBM treated with chemotherapy and radiation alone [21].

Capillary Heterogeneity Imaging

Extensions of current pharmacokinetic modeling approaches have also been developed for DRCE-MRI. St Lawrence et al. extended their original adiabatic tissue heterogeneity model to provide spatial maps of tumor blood flow (F), extraction fraction (E), permeability–surface area product (PS), transfer constant (K^{trans}), washout rate (k_{ep}), interstitial volume (V_e), blood volume (V_b), capillary transit time (t_c), and capillary heterogeneity (a^{-1}) [22]. This has been termed the gamma capillary transit time (GCTT) model, and the introduction of the capillary transit time and heterogeneity terms represents novel biomarkers that could provide new evidence about microvascular structure. Jensen et al. [23] applied the model in a group of patients with glioblastoma and found close correlation between the capillary transit time, HIF-1, and VEGF expression in active tumor. Furthermore, patient survival correlated with only two DCE parameters: capillary

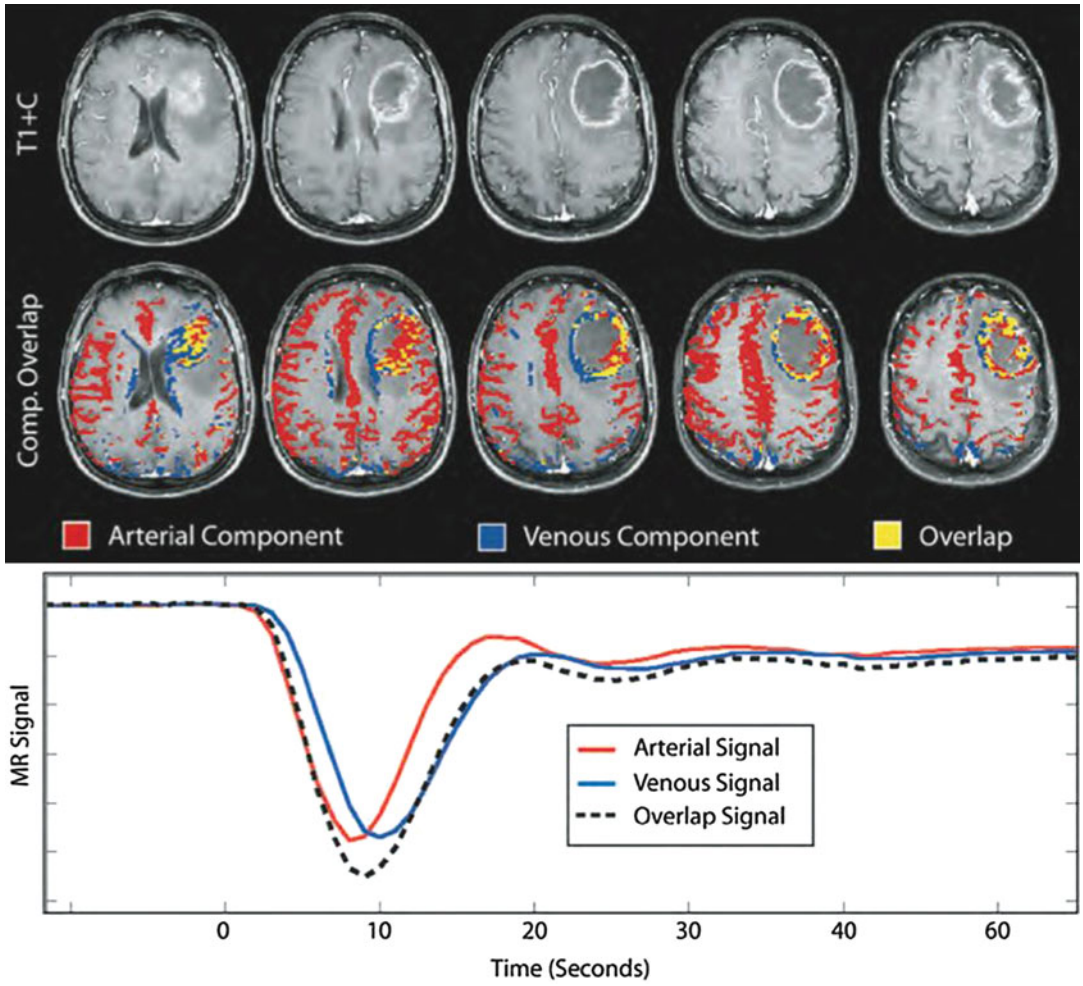

Fig. 5 Example of Avol in a representative case of untreated GBM. (*Top*) Row 1 shows a series of T1-WI postcontrast images, and row 2 shows the same series with the arterial (*red*) and venous (*blue*) ICA components overlaid. The overlap of the two is indicated in *yellow*. (*Bottom*) Mean MR signal within voxels defined by ICA components and the overlap (From Ref. [24] with permission)

heterogeneity in active tumor and interstitial volume in areas of peri-tumoral edema.

Arteriovenous Overlap Imaging (AVOL)

La Violette et al. [24] studied a group of 43 patients with high-grade glioma using independent component analysis to separate the vasculature into arterial and venous components. They observed that the abnormal vascular flow patterns in tumors gave rise to a number of voxels that were classified both as arterial and venous (Fig. 5).

They used this arteriovenous overlap (AVOL) as an index of abnormal tumor microvasculature, showing that median survival was greater in patients where the Avol decreased in response to bevacizumab treatment. They propose the Avol as an independent biomarker of abnormal microvascular hemodynamics. In a subsequent study the same authors demonstrated significant sensitivity of the Avol measurement to contrast leakage and modify their recommendations to suggest that the measurement should be performed on a second dose of contrast following a preloading dose to saturate the T1 effects of contrast leakage [25].

Imaging Hypoxia Using MRI

Hypoxia plays a central role in tumor development, angiogenesis, tumor growth, and resistance to treatment. Hypoxia is intimately related to the structure and function of the vascular microenvironment. Inadequate supply of oxygen and other nutrients to tumor cells and to tumor support and inflammatory cells results in local hypoxia and which forms one of the main pro-angiogenic stimuli. Likewise, failure of angiogenesis to keep pace with the rate of tumor proliferation or metabolism will give rise to areas of hypoxic tissue within the tumor. The presence of hypoxia has a profound effect on tumor biology and has been shown to correlate with the probability of metastatic spread, tumor recurrence, resistance to chemotherapy and radiotherapy, invasive phenotype, and decreased patient survival. It is clear that prolonged or severe hypoxia induces phenotypic changes such as loss of genotype stability, loss of apoptotic potential, and oncogene activation. Imaging methods for the identification of hypoxic tissue have classically relied on the use of positron emission tomography (*vide infra*). However, there is increasing interest in the use of MR-based techniques to identify areas of hypoxic tissue. As described in the previous section, VAI has been shown to allow measurement of regional oxygen consumption although the biomarker has not yet been fully biologically qualified. Similarly, capillary heterogeneity imaging demonstrates close correlation with the expression of HIF-1.

Over the past several years, susceptibility-weighted imaging (SWI) has become part of routine neuroimaging. SWI is used to detect magnetic susceptibility of different tissues and is now clinically used to assess neoplastic microvascular, microbleeds and necrotic areas. One potential cause of increased signal on SWI is the presence of increasing concentrations of deoxyhemoglobin providing another potential IB for hypoxic tissue. In a recent study, 64 patients with brain tumors underwent SWI demonstrating that R2* values were significantly different between low-grade and high-grade glioma. The authors suggest that the R2* value may reflect alterations in deoxygenated hemoglobin which are higher in high-grade than low-grade glioma [26] (Fig. 6).

However, although these signal changes may have some diagnostic value, they have not been biologically qualified as an IB of tissue hypoxia, and it is clear that the signal would also be affected by other causes of susceptibility contrast such as calcification or microhemorrhage.

Attempts to qualify the presence of hypoxia using T1-WI oxygen-enhanced magnetic resonance imaging (OE-MRI) measurements have recently been described [27]. These and previous works have demonstrated that increasing the concentration of inspired oxygen produces a signal detectable in blood and tissues on T1-WI imaging. Animal models of the area under the curve resulting from oxygen enhancement showed positive correlation with histologically demonstrated hypoxic tissue and a negative correlation with vessel density (Fig. 7).

These relationships were not seen with parameters derived from DCE-MRI measurements. Clinical data confirm that the same changes were seen in patients with glioblastoma apparently identifying central areas of hypoxic tissue. The use of T1-WI dynamic imaging together with oxygen enhancement appears highly promising although further biological and technical validation is still required .

Molecular Imaging of the Tumor Vascular Microenvironment

Understanding of the tumor vascular microenvironment and of the angiogenic process continues to increase at an almost exponential rate. Enormous investment leads to the ongoing identification of numerous novel therapeutic targets and candidate compounds which will pass into preclinical and, eventually, for the more successful agents, into clinical trial. Although dynamic contrast-enhanced imaging methods have provided, and continue to provide, the mainstay of imaging biomarker support for such studies, they describe only selected elements of the tumor microvascular environment. There is a growing demand for biomarkers that can quantify specific molecular processes to provide a more comprehensive toolkit for the investigation of the TVM

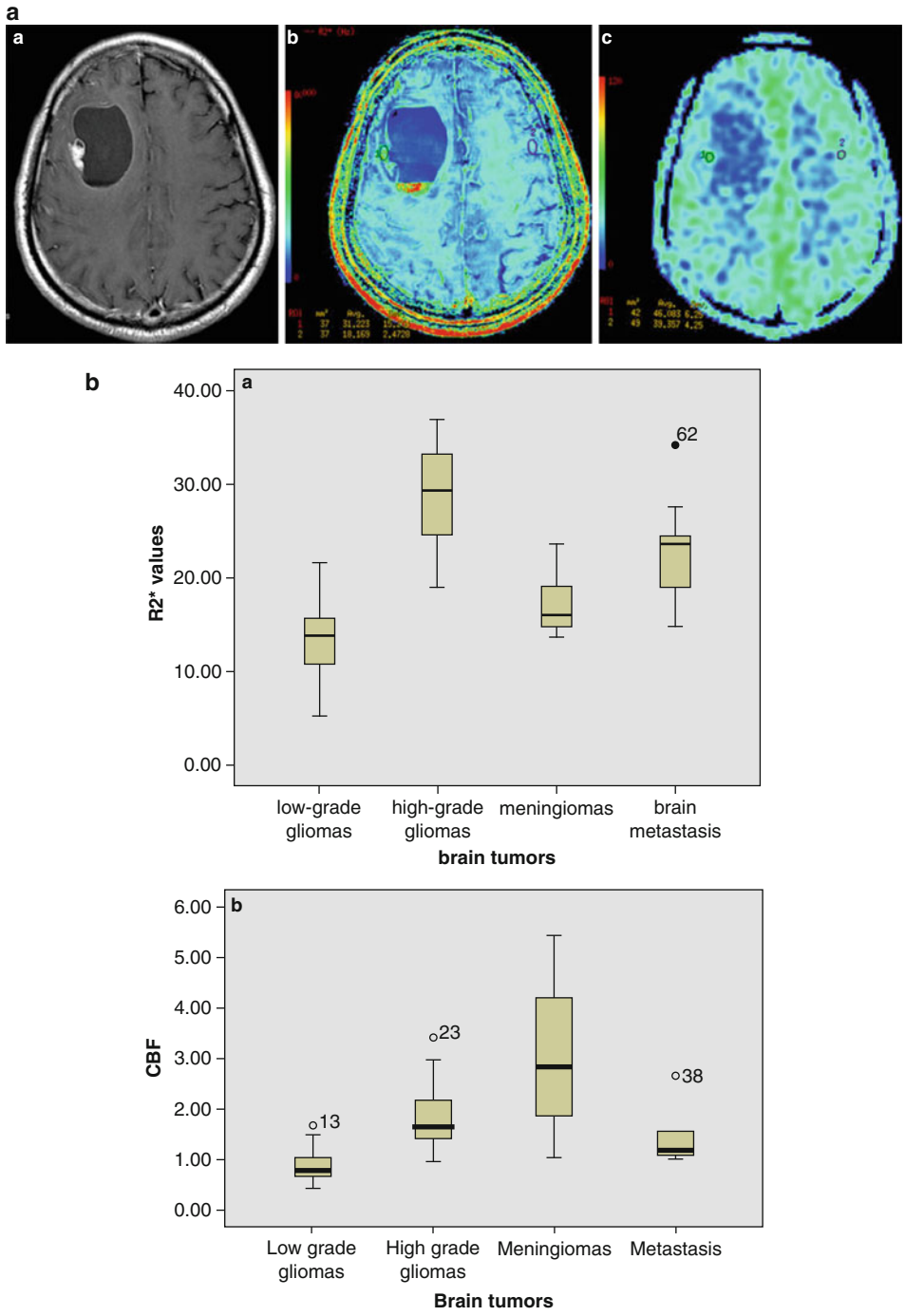

Fig. 6 (**a**) A 46-year-old man with a histologically proven glioblastoma multiforme (grade IV) located in the right frontal lobe. (**a**) Axial T1-WI postcontrast image demonstrates nodular enhancement in the tumor. (**b**) The R2* map shows an area of high R2* values (31.22) in the tumor. There is hemorrhage at the bottom of the tumor. (**c**) The ASL CBF map demonstrates nodular hyperperfusion. **b** R2* and rCBF values of four types of brain tumors. (**a**) The decreasing order of R2* values is high-grade gliomas, brain metastasis, meningiomas, and low-grade gliomas. (**b**) The sequence rCBF values are meningiomas, high-grade gliomas, brain metastasis, and low-grade gliomas (From Ref. [26] with permission)

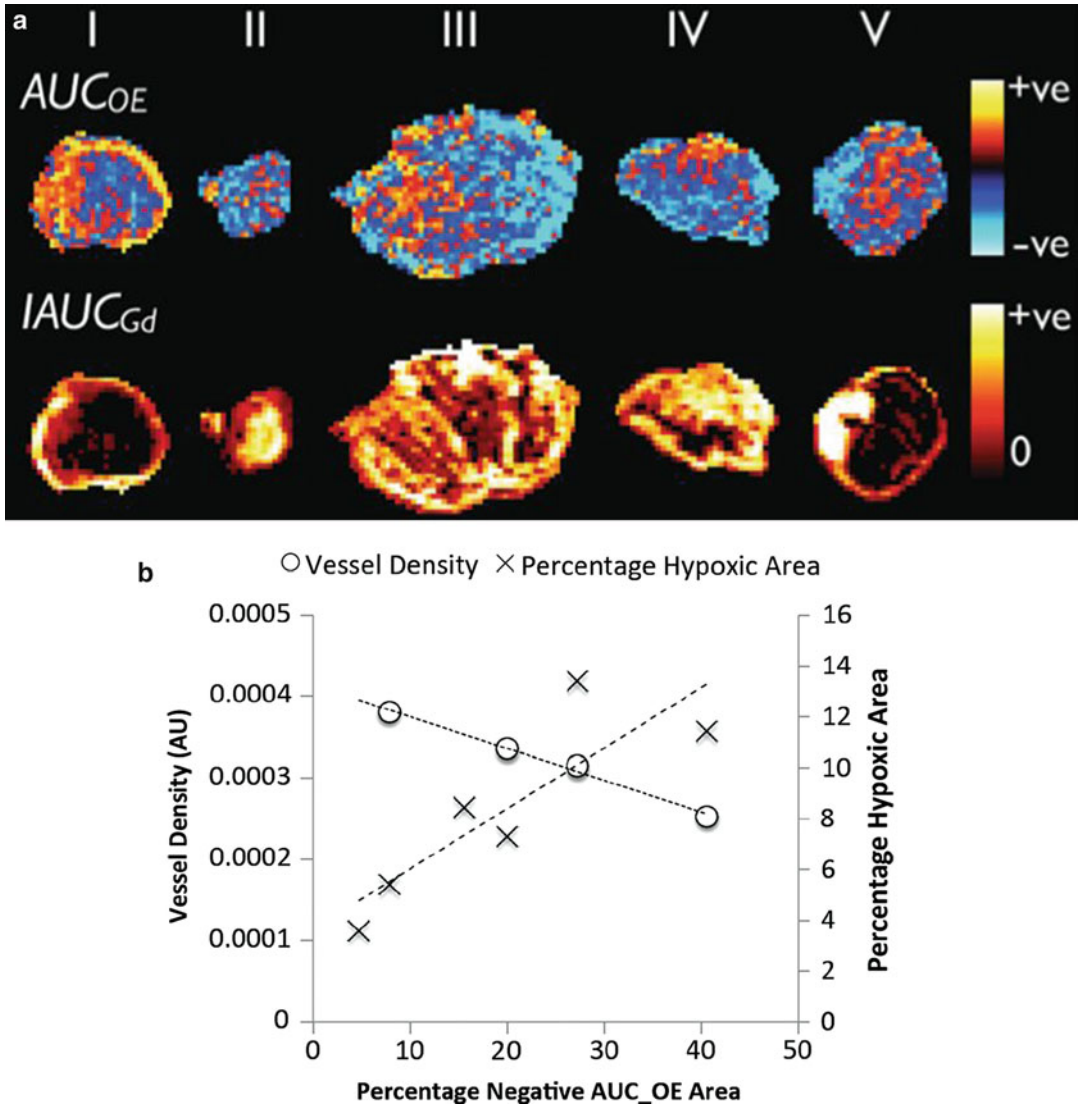

Fig. 7 (**a**) Tumors from five patients with GBM. *Top row*: area under the DR1 curve for OE-MRI, AUC_{OE} displayed using a hot color scale for positive values and negative values using a cool color scale. All images windowed to maximize visible dynamic range symmetrically around zero AUC_{OE} change. *Bottom row*: area under the DR1 curve for DCE-MRI, $IAUC_{Gd}$ displayed using a hot color scale with all images windowed to maximize visible dynamic range. Numerals indicate patient tumor index. (**b**) Correlation between negative AUCOE areas following oxygen inhalation with vessel density (*circles*) and percentage hypoxic area (*crosses*) in all U87MG tumors (From Ref. [27] with permission)

and of angiogenesis, antiangiogenic, and antivascular therapies. This has led to the development of a number of novel radiotracers, principally designed for use with positron emission tomography (PET), which target molecules expressed by vascular and vascular support cells. Many candidate tracers are currently in development and have been used for preclinical studies. For a review of the current state-of-the-art in this field, the reader is directed toward a number of major review articles. In many cases the focus of these agents is on systemic tumors, and there has

been little application in brain tumors in humans. The main area of interest with regard to human glioma has been around imaging of hypoxia and integrin expression.

Imaging Hypoxia Using PET

PET imaging is an ideal modality for evaluating hypoxia. The PET imaging agent fluoromisonidazole (18F-FMISO) is an 18F fluorinated derivative of misonidazole, an azomycin hypoxic cell sensitizer. It binds covalently to intracellular molecules at a rate inversely proportional to intracellular O_2 concentration. 18F-FMISO diffuses freely across the blood–brain barrier and is reduced at any hypoxic site where it is not excreted or highly metabolized and its metabolites have a rapid plasma clearance, so normalization for delivery is not required. Quantitatively, the degree of hypoxia can be defined by hypoxic fraction or volume or can be expressed by its severity, defined as the region with the lowest oxygen concentration, and its relative level. 18F-FMISO imaging studies cannot provide values of regional oxygen concentration, but the maximum tumor/blood ratio is a convenient surrogate for the worst level of hypoxia in the image. 18F-FMISO is currently the most widely used positron emission tomography (PET) imaging agent for hypoxia. The imaging procedure is a well-tolerated procedure by patients and imaging takes around 20–30 min, starting from 75 to 150 min after injection.

18F-FMISO has been validated in several animal models and human disease conditions, and its signal is independent of other factors associated with hypoxia, such as regional glucose concentration, glutathione levels, other transporters, and pH.

In 3 studies of 34 patients with glioma, only glioblastoma demonstrated constant uptake of 18F-FMISO, whereas neither low-grade glioma nor anaplastic astrocytoma showed this effect. A recent study in GBM patients, imaged preoperatively using 18F-FMISO, showed positive correlations between relative hypoxia (defined as the ratio of the hypoxic volume to the MRI T2-defined tumor volume) and the net rate of cell proliferation, as well as between the biological aggressiveness ratio (defined as the ratio between the net rate of cell proliferation and the net rate of invasion) and relative hypoxia, scaled to the blood activity of the tracer.

18F-FMISO and 15O-H2O PET have also been used in brain tumors to provide matched measures of tumor hypoxia and perfusion. Increased 18F-FMISO brain tumor retention was observed in GBM (seven out of seven) and was associated with an increased 18F-FMISO tumor distribution volume, which was also used as a quantitative criterion for hypoxia. 18F-FMISO accumulated in both hypo- and hyperperfused tumor regions, suggesting that hypoxia in glioblastoma may develop irrespective of the magnitude of perfusion [28]. Other studies have demonstrated correlations between 18F-FMISO uptake and expression of vascular endothelial growth factor (VEGF)-R1 and Ki67 expression in glioblastomas and a relationship between the uptake volume and intensity and both tumor progression and overall survival (Fig. 8).

Relatively poor tumor-to-background ratios combined with slow clearance from normal tissue have led to the ongoing search for improved hypoxia imaging agents. For a fuller review of the potential advantages and disadvantages of these alternate imaging agents, the reader is directed to a number of comprehensive review articles.

Imaging Integrin Expression

Integrins are membrane receptors comprised of an α and a β subunit that mediate interactions between cells. To date, 18 different α and 8 different β subunits have been identified, forming 24 different integrin receptors [29]. A common property of many integrins is their interaction with the arginine-glycine-aspartic acid (RGD) sequence found in extracellular matrix proteins like vitronectin, fibrinogen, thrombospondin, and fibronectin. The most extensively studied of these in the angiogenic process is the integrin αvβ3

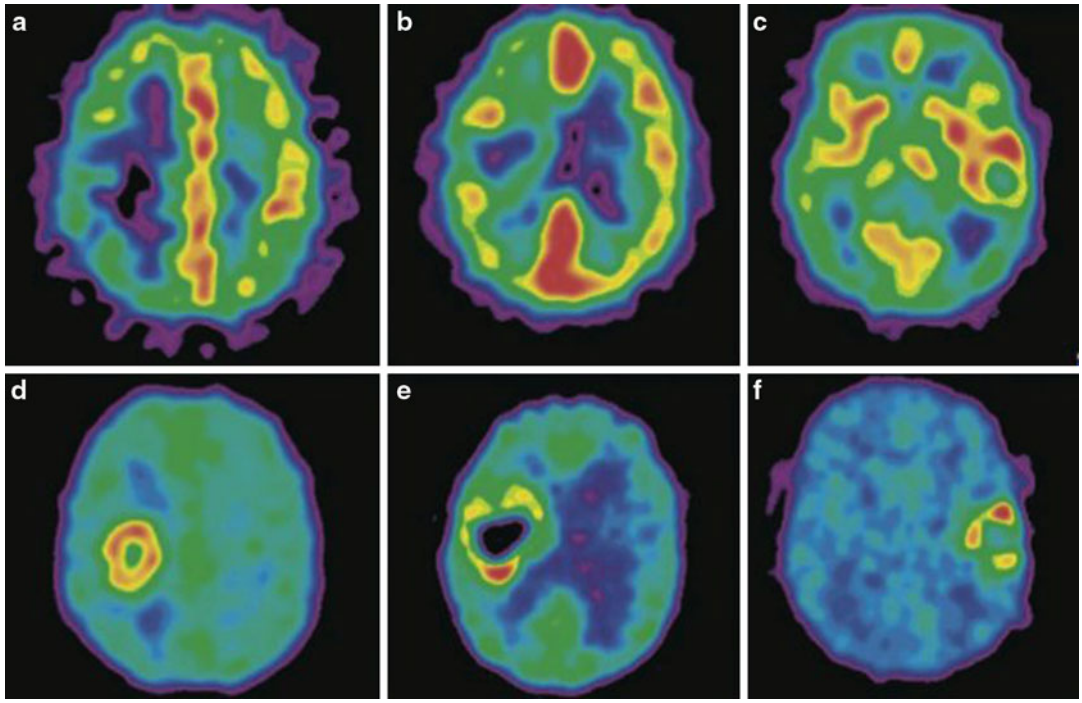

Fig. 8 (**a**–**c**) ^{15}O-H2O PET perfusion images in three patients with glioblastoma multiforme. (**d**–**f**) Corresponding late 18F-FMISO PET images show tumor hypoxia in low perfusion, in intermediate perfusion with an inverse pattern compared with hypoxia, and in high perfusion. PET images are normalized to their own maximum (From Ref. [28] with permission)

which is highly expressed on the surface of activated EC. However, integrins are commonly expressed on the surface of tumor cells, and the interpretation of the signal obtained from integrin imaging can therefore be complex [30]. The first integrin-specific PET tracer used in humans was [18F]Galacto-RGD. The initial study of mixed tumor types demonstrated wide variability of tumor uptake with high background in the kidneys, liver, spleen, and bowel. Immunohistological examination of resected tissue demonstrated that the number of αvβ3-positive vessels per field of view correlated highly with tumor uptake of [18F]Galacto-RGD [31]. A similar correlation between uptake and immunohistochemical staining was also demonstrated in a later, larger study. In glial cell tumors there was moderate but variable uptake, most marked in areas of high proliferation or tumor infiltration. Immunohistochemical staining was positive both in EC and in tumor cells, and tracer uptake correlated with immunohistochemical assays of αvβ3 integrin expression [32] (Fig. 9).

A number of modifications designed to improve the pharmacokinetic properties of RGD peptides have been described, including the development of multimeric tracers designed to more effectively identify tumors in areas of high physiologic integrin expression. Direct comparison of monomeric, dimeric, and tetrameric cyclic RGD tracers conjugated with DOTA and radiolabeled with ^{111}In in mice with SK-RC-52 renal cell carcinoma xenografts demonstrated tumor uptake of the tetramer which exceeded that of both the dimer and the monomer [34], and a 64Cu-DOTA-RGD octamer demonstrated higher uptake than tetramer versions in human glioblastoma tumor grafts [35].

One significant alternate integrin-specific tracer is [18F]-fluciclatide, which has been developed by GE Healthcare and is becoming widely available. This commercially available tracer

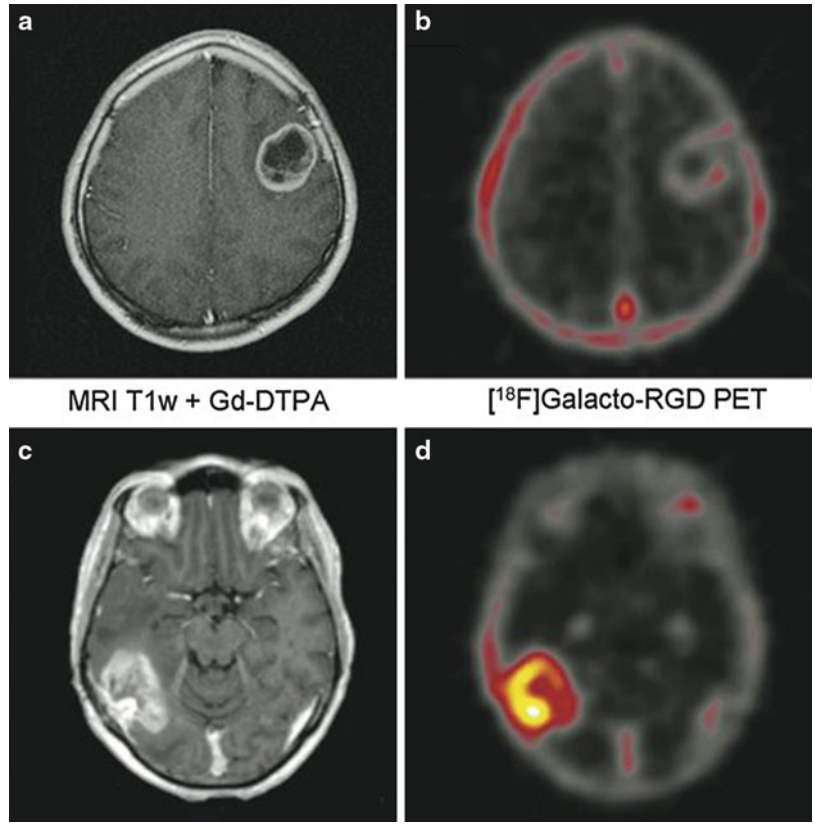

Fig. 9 Examples of patients with glioblastoma multiforme of the left frontal lobe (**a**, **b**) and right parieto-occipital lobe (**c**, **d**). Note the intense peripheral enhancement in the gadolinium-DTPA-enhanced MRI scans in both tumors (**a**, **c**). However, the tumor in (**b**) shows only very faint tracer uptake in the [18F]Galacto-RGD PET (maximum standardized uptake value [SUVmax], 1.2), whereas the tumor in (**d**) demonstrates substantially more intense [18F]Galacto-RGD uptake (SUVmax, 2.8) (From Ref. [33] with permission)

shows different binding affinities with the highest affinity for $\alpha_v\beta_5$ (IC_{50} 0.1 nM) followed by integrin $\alpha_v\beta_3$ (IC_{50} 11.1 nM). A study in human glioma heterografts treated with sunitinib demonstrated a therapy-induced reduction in tumor uptake over a 2-week period. This correlated with a reduction in tumor MVD suggesting that this agent is capable of demonstrating vascular responses to transgenic inhibition prior to the occurrence of significant volumetric changes [36].

The potential role of integrin imaging in the clinical environment remains uncertain. Observations of associations between integrin expression and tumor progression in melanoma and tumor grade in sarcoma have suggested potential clinical utility. Similarly, preclinical studies have demonstrated that integrin αvβ3 has an important role in promoting aggression and metastatic potential in breast cancer and glioma. These observations suggest specific potential clinical utility for integrin imaging, particularly in the selection of patients for antiangiogenic therapies.

Clinical Applications of Microvascular Imaging

The use of IB microvascular structure and function has been the subject of extensive clinical research, and some better-characterized IB are now passing into routine clinical use. Since much of the development of DCE-MRI techniques occurred in the brain, a number of these have now been shown to have actual or potential neuro-oncological application.

Diagnosing Glioma Mimics

In a large series of 5,000 stereotactic biopsies, only 64.4 % were glioma, and it remains true, despite improvements in routine clinical imaging, that these lesions cannot always be confidently diagnosed. DCE-MRI techniques have been shown to allow improved differentiation between

glial cell tumors and common diagnostic mimics. Distinguishing solitary metastases from high-grade glioma can be difficult; however, several studies have shown that rCBV values are higher in GBM particularly in the region surrounding the malignant tumor [9]. This has been attributed to the presence of mixed vasogenic and cytotoxic edema due to tumor cell invasion around the margins of GBM. The diagnosis of cerebral lymphoma is also greatly strengthened by the low rCBV values that these tumors exhibit, clearly distinguishing them from GBM which shows high rCBV despite very similar enhancement patterns on contrast-enhanced static images [37]. Another major differential diagnosis of GBM is cerebral abscess. Abscess may have very similar classical imaging appearances but is of course an important urgent medical diagnosis. Once again rCBV in the rim of an enhancing access is found to be significantly lower than that seen in HGG [38]. Although there is significant overlap between these groups, diagnostic sensitivity and specificity become very high when combined with measurements of apparent diffusion coefficient from diffusion-weighted imaging, which demonstrates restricted diffusion in the glial tumors [38].

Grading Glioma

Many studies have described variations in DCE-MRI-derived biomarkers between different grades of glioma [39]. To a large extent this is an interesting biological validation of the imaging biomarker but represents little or no clinical benefit in the management of the patient. In all cases tissue will be obtained and tissue diagnosis will be made, which remains, at the present time, the gold standard diagnostic criteria [40]. Typically studies show increases in angiogenic activity, proportionate to increasing aggressiveness and grade of the tumor. Multiple authors have reported increases in rCBV related to grade, capable of differentiating low-grade from high-grade glioma [41]. Some authors have also demonstrated similar correlations between grade and vascular fraction from DRCE-MRI although it is noteworthy that differentiation between grade III and grade IV glioma is unreliable with either technique.

Identification of areas of dedifferentiation in low-grade tumors and of aggressive areas in HGG, particularly grade III, avoids erroneous undergrading of the tumor due to failure to sample the most aggressive component. In many clinical practices this has led to routine use of rCBV maps to identify optimal sites for biopsy.

Identifying Transformation in Low-Grade Glioma

Low-grade glioma has a propensity to undergo malignant transformation, but the time scale is highly variable between individuals. Monitoring of patients with low-grade disease is aimed at identifying transformation at an early stage and has classically relied on the development of contrast enhancement within the tumor. Contrast enhancement can result from contrast leakage due to increased endothelial permeability or from increased intravascular contrast due to increased proportional blood volume. Measurement of increased rCBV using the DSCE-MRI has been shown to allow early detection of dedifferentiation by 6–12 months compared with conventional imaging and is now in common clinical use [42].

Distinguishing Recurrent Tumor from Treatment Effects

Following chemoradiotherapy there is a significant incidence of apparent progression of the tumor on conventional radiological criteria that later resolves. This is referred to as pseudo-progression and can cause significant problems with management and treatment planning. The pseudo-progression syndrome appears to result from leakiness of endothelial membranes due to vascular damage following chemoradiotherapy. The incidence of pseudo-progression has been reported as 9 % with radiation alone and 21–31 % with concomitant temozolomide. Routine MRI sequences are unable to distinguish between

true progression and early or late related treatment effects. Pseudo-progression is characterized on DSCE-MRI by lower rCBV, lower relative peak height of the enhancement curve, and higher percentage signal recovery compared to recurrent tumor [43]. However, although some investigators have showed extremely high discriminative power of rCBV alone, others have failed to achieve this despite the use of multimodality IB including MR spectroscopy and ADC measurements [43].

In the late stages following chemoradiotherapy, radiation necrosis may occur between 4 and 12 months after radiation. It is related to the areas of highest radiation dose and also causes significant problems with treatment planning. In one study, 51 % of patients with radiological evidence of glioma progression following temozolomide were found to have radiation necrosis following surgical resection with no evidence of recurrent tumor. Microvascular IB, particularly CBV, show differences between radiation necrosis and recurrent tumor, being higher in tumor, but these are not sufficiently great to allow confident diagnosis [44]. In one study sensitivity and specificity were 83.3 % and 100 %, respectively. More recently Larsen et al. reported sensitivities and specificities of 100 % in a small study of 14 patients [45]; however, these levels of accuracy have not been repeated in larger studies. Although DSCE-MRI may help make the differential diagnosis, it is clear that the microvascular imaging biomarkers are not yet sufficiently discriminative to be used alone.

Predicting Treatment Response

Many groups have demonstrated a relationship between progression-free survival and/or overall survival and IB describing the TVM. As early as 2006 it was shown that glioma patients with higher proportions of high rCBV had reduced prognosis. Furthermore these workers showed that changes in tumor CBV during the early treatment course also predicted for survival. Better survival was predicted by a decrease in the fractional low-CBV tumor volume at week 1 of RT vs. before RT and by a decrease in the fractional high-CBV tumor volume at week 3 vs. week 1 [46]. These findings have been confirmed by a number of other similar studies. Furthermore, rCBV following resection has also been shown to be predictive of overall survival in patients with cerebral metastases.

Summary

Despite an explosion of research concerning the biology of the TVM, knowledge of the subject continues to increase exponentially as the drive for new anticancer therapeutics continues. The availability of minimally invasive, accurate, reproducible IB forms a major component of that research drive. The past 20 years has seen the development and evolution of sophisticated image acquisition and analysis techniques aimed at developing IB which address the most relevant components of disease physiology and which are truly able to provide important information of direct relevance. A vast amount of development continues to occur around dynamic contrast-enhanced methodologies, which have now become ubiquitous in drug discovery and drug trials for a large range of antiangiogenic and vascular targeting agents. Increasingly we are seeing these biomarkers being used in clinic although there remains a very significant delay between the initial biological validations of novel IB in their eventual clinical qualification.

Despite major strides there are enormous challenges ahead. Although the development of IB has been almost exponential in nature, there are significant and growing anxieties about the complexity of utilizing IB across multiple centers and in large-scale studies. A number of international initiatives are currently under way to try and standardize acquisition and analysis techniques and to improve both technical and biological validation and qualification strategies. This process of consolidation will continue in parallel with innovation because, although IB are expensive and challenging to utilize, they offer many unique properties and unparalleled advantages for the study of tumor biology.

References

1. Hanahan D, Weinberg RA (2000) The hallmarks of cancer. Cell 100(1):57–70
2. Patan S (2004) Vasculogenesis and angiogenesis. Cancer Treat Res 117:3–32
3. Carmeliet P, Jain RK (2011) Molecular mechanisms and clinical applications of angiogenesis. Nature 473(7347):298–307
4. Cheng SY, Huang HJ, Nagane M, Ji XD, Wang D, Shih CC et al (1996) Suppression of glioblastoma angiogenicity and tumorigenicity by inhibition of endogenous expression of vascular endothelial growth factor. Proc Natl Acad Sci U S A 93(16):8502–8507
5. Chen HX, Cleck JN (2009) Adverse effects of anticancer agents that target the VEGF pathway. Nat Rev Clin Oncol 6(8):465–477
6. Nico B, Benagiano V, Mangieri D, Maruotti N, Vacca A, Ribatti D (2008) Evaluation of microvascular density in tumors: pro and contra. Histol Histopathol 23(5):601–607
7. Yao WW, Zhang H, Ding B, Fu T, Jia H, Pang L et al (2011) Rectal cancer: 3D dynamic contrast-enhanced MRI; correlation with microvascular density and clinicopathological features. Radiol Med 116(3):366–374
8. Jackson A, Kassner A, Annesley-Williams D, Reid H, Zhu XP, Li KL (2002) Abnormalities in the recirculation phase of contrast agent bolus passage in cerebral gliomas: comparison with relative blood volume and tumor grade. AJNR Am J Neuroradiol 23(1):7–14
9. Cha S, Lupo JM, Chen MH, Lamborn KR, McDermott MW, Berger MS et al (2007) Differentiation of glioblastoma multiforme and single brain metastasis by peak height and percentage of signal intensity recovery derived from dynamic susceptibility-weighted contrast-enhanced perfusion MR imaging. AJNR Am J Neuroradiol 28(6):1078–1084
10. Thacker NA, Scott ML, Jackson A (2003) Can dynamic susceptibility contrast magnetic resonance imaging perfusion data be analyzed using a model based on directional flow? J Magn Reson Imaging 17(2):241–255
11. Jackson A, Li KL, Zhu X (2014) Semi-quantitative parameter analysis of DCE-MRI revisited: monte-carlo simulation, clinical comparisons, and clinical validation of measurement errors in patients with type 2 neurofibromatosis. PLoS One 9(3):e90300
12. Jackson A (2004) Analysis of dynamic contrast enhanced MRI. Br J Radiol 77(Spec No 2):S154–S166
13. O'Connor JP, Jackson A, Parker GJ, Roberts C, Jayson GC (2012) Dynamic contrast-enhanced MRI in clinical trials of antivascular therapies. Nat Rev Clin Oncol 9(3):167–177
14. Tofts PS, Kermode AG (1991) Measurement of the blood-brain barrier permeability and leakage space using dynamic MR imaging. 1. Fundamental concepts. Magn Reson Med 17(2):357–367
15. Leach MO, Brindle KM, Evelhoch JL, Griffiths JR, Horsman MR, Jackson A et al (2005) The assessment of antiangiogenic and antivascular therapies in early-stage clinical trials using magnetic resonance imaging: issues and recommendations. Br J Cancer 92(9):1599–1610
16. Naish JH, McGrath DM, Bains LJ, Passera K, Roberts C, Watson Y et al (2011) Comparison of dynamic contrast-enhanced MRI and dynamic contrast-enhanced CT biomarkers in bladder cancer. Magn Reson Med 66(1):219–226
17. Jain RK (2001) Normalizing tumor vasculature with anti-angiogenic therapy: a new paradigm for combination therapy. Nat Med 7(9):987–989
18. Schmainda KM, Rand SD, Joseph AM, Lund R, Ward BD, Pathak AP et al (2004) Characterization of a first-pass gradient-echo spin-echo method to predict brain tumor grade and angiogenesis. AJNR Am J Neuroradiol 25(9):1524–1532
19. Batchelor TT, Sorensen AG, di Tomaso E, Zhang WT, Duda DG, Cohen KS et al (2007) AZD2171, a pan-VEGF receptor tyrosine kinase inhibitor, normalizes tumor vasculature and alleviates edema in glioblastoma patients. Cancer Cell 11(1):83–95
20. Sorensen AG, Batchelor TT, Zhang WT, Chen PJ, Yeo P, Wang M et al (2009) A "vascular normalization index" as potential mechanistic biomarker to predict survival after a single dose of cediranib in recurrent glioblastoma patients. Cancer Res 69(13):5296–5300
21. Emblem KE, Mouridsen K, Bjornerud A, Farrar CT, Jennings D, Borra RJ et al (2013) Vessel architectural imaging identifies cancer patient responders to anti-angiogenic therapy. Nat Med 19(9):1178–1183
22. St Lawrence K, Verdecchia K, Elliott J, Tichauer K, Diop M, Hoffman L et al (2013) Kinetic model optimization for characterizing tumour physiology by dynamic contrast-enhanced near-infrared spectroscopy. Phys Med Biol 58(5):1591–1604
23. Jensen RL, Mumert ML, Gillespie DL, Kinney AY, Schabel MC, Salzman KL (2014) Preoperative dynamic contrast-enhanced MRI correlates with molecular markers of hypoxia and vascularity in specific areas of intratumoral microenvironment and is predictive of patient outcome. Neuro Oncol 16(2):280–291
24. LaViolette PS, Cohen AD, Prah MA, Rand SD, Connelly J, Malkin MG et al (2013) Vascular change measured with independent component analysis of dynamic susceptibility contrast MRI predicts bevacizumab response in high-grade glioma. Neuro Oncol 15(4):442–450
25. LaViolette PS, Daun MK, Paulson ES, Schmainda KM (2014) Effect of contrast leakage on the detection of abnormal brain tumor vasculature in high-grade glioma. J Neurooncol 116(3):543–549
26. Liu Z, Liao H, Yin J, Li Y (2014) Using R2* values to evaluate brain tumours on magnetic resonance imaging: preliminary results. Eur Radiol 24(3):693–702
27. Linnik IV, Scott ML, Holliday KF, Woodhouse N, Waterton JC, O'Connor JP et al (2013) Noninvasive

tumor hypoxia measurement using magnetic resonance imaging in murine U87 glioma xenografts and in patients with glioblastoma. Magn Reson Med
28. Bruehlmeier M, Roelcke U, Schubiger PA, Ametamey SM (2004) Assessment of hypoxia and perfusion in human brain tumors using PET with 18F-fluoromisonidazole and 15O-H_2O. J Nucl Med 45(11):1851–1859
29. Takada Y, Ye X, Simon S (2007) The integrins. Genome Biol 8(5):215
30. Desgrosellier JS, Cheresh DA (2010) Integrins in cancer: biological implications and therapeutic opportunities. Nat Rev Cancer 10(1):9–22
31. Haubner R, Kuhnast B, Mang C, Weber WA, Kessler H, Wester HJ et al (2004) [18F]Galacto-RGD: synthesis, radiolabeling, metabolic stability, and radiation dose estimates. Bioconjug Chem 15(1):61–69
32. Schittenhelm J, Schwab EI, Sperveslage J, Tatagiba M, Meyermann R, Fend F et al (2013) Longitudinal expression analysis of alpha v integrins in human gliomas reveals upregulation of integrin alpha v beta 3 as a negative prognostic factor. J Neuropathol Exp Neurol 72(3):194–210
33. Schnell O, Krebs B, Carlsen J, Miederer I, Goetz C, Goldbrunner RH et al (2009) Imaging of integrin alpha (v)beta(3) expression in patients with malignant glioma by [18F] Galacto-RGD positron emission tomography. Neuro Oncol 11(6):861–870
34. Liu S, Hsieh WY, Jiang Y, Kim YS, Sreerama SG, Chen X et al (2007) Evaluation of a (99m)Tc-labeled cyclic RGD tetramer for noninvasive imaging integrin alpha(v)beta3-positive breast cancer. Bioconjug Chem 18(2):438–446
35. Li ZB, Cai W, Cao Q, Chen K, Wu Z, He L et al (2007) (64)Cu-labeled tetrameric and octameric RGD peptides for small-animal PET of tumor alpha(v)beta (3) integrin expression. J Nucl Med 48(7):1162–1171
36. Battle MR, Goggi JL, Allen L, Barnett J, Morrison MS (2011) Monitoring tumor response to antiangiogenic sunitinib therapy with 18F-fluciclatide, an 18F-labeled alphaVbeta3-integrin and alphaV beta5-integrin imaging agent. J Nucl Med 52(3):424–430
37. Calli C, Kitis O, Yunten N, Yurtseven T, Islekel S, Akalin T (2006) Perfusion and diffusion MR imaging in enhancing malignant cerebral tumors. Eur J Radiol 58(3):394–403
38. Erdogan C, Hakyemez B, Yildirim N, Parlak M (2005) Brain abscess and cystic brain tumor: discrimination with dynamic susceptibility contrast perfusion-weighted MRI. J Comput Assist Tomogr 29(5):663–667
39. Patankar TF, Haroon HA, Mills SJ, Baleriaux D, Buckley DL, Parker GJ et al (2005) Is volume transfer coefficient (K(trans)) related to histologic grade in human gliomas? AJNR Am J Neuroradiol 26(10):2455–2465
40. Thompson G, Mills SJ, Stivaros SM, Jackson A (2010) Imaging of brain tumors: perfusion/permeability. Neuroimaging Clin N Am 20(3):337–353
41. Yoon JH, Kim JH, Kang WJ, Sohn CH, Choi SH, Yun TJ et al (2014) Grading of cerebral glioma with multiparametric MR imaging and 18F-FDG-PET: concordance and accuracy. Eur Radiol 24(2):380–389
42. Law M, Young RJ, Babb JS, Peccerelli N, Chheang S, Gruber ML et al (2008) Gliomas: predicting time to progression or survival with cerebral blood volume measurements at dynamic susceptibility-weighted contrast-enhanced perfusion MR imaging. Radiology 247(2):490–498
43. Di Costanzo A, Scarabino T, Trojsi F, Popolizio T, Bonavita S, de Cristofaro M (2014) Recurrent glioblastoma multiforme versus radiation injury: a multiparametric 3-T MR approach. Radiol Med 119:616–624
44. Sugahara T, Korogi Y, Tomiguchi S, Shigematsu Y, Ikushima I, Kira T et al (2000) Posttherapeutic intraaxial brain tumor: the value of perfusion-sensitive contrast-enhanced MR imaging for differentiating tumor recurrence from nonneoplastic contrast-enhancing tissue. AJNR Am J Neuroradiol 21(5):901–909
45. Larsen VA, Simonsen HJ, Law I, Larsson HB, Hansen AE (2013) Evaluation of dynamic contrast-enhanced T1-weighted perfusion MRI in the differentiation of tumor recurrence from radiation necrosis. Neuroradiology 55(3):361–369
46. Cao Y, Tsien CI, Nagesh V, Junck L, Ten Haken R, Ross BD et al (2006) Survival prediction in high-grade gliomas by MRI perfusion before and during early stage of RT [corrected]. Int J Radiat Oncol Biol Phys 64(3):876–885